# Protein resonance assignment by solid-state NMR based on $^{1}$H-detected $^{13}$C-based double-quantum spectroscopy at fast MAS

Alons Lends[1*], Mélanie Berbon[1], Birgit Habenstein[1], Yusuke Nishiyama[2*], Antoine Loquet[1*]

[1] CNRS, Chemistry and Biology of Membranes and Nanoobjects (CBMN) UMR 5348, Institut Europeen de Chimie et Biologie (IECB), University of Bordeaux, F-33600 Pessac, France

[2] RIKEN-JEOL Collaboration Center, RIKEN, Yokohama, Kanagawa 230-0045, Japan, and JEOL RESONANCE Inc., 3-1-2 Musashino, Akishima, Tokyo 196-8558, Japan

*corresponding authors: A. Lends (a.lends@iecb.u-bordeaux.fr), Y. Nishiyama (yunishiy@jeol.co.jp) and A. loquet (a.loquet@iecb.u-bordeaux.fr).

**Abstract**

Solid-state NMR spectroscopy is a powerful technique to study insoluble and non-crystalline proteins and protein complexes at atomic resolution. The development of proton ($^{1}$H) detection at fast magic-angle spinning (MAS) has considerably increased the analytical capabilities of the technique, enabling the acquisition of $^{1}$H-detected fingerprint experiments in few hours. Here an approach based on double-quantum (DQ) $^{13}$C spectroscopy, detected on $^{1}$H, is introduced at fast MAS (70 kHz) to perform the sequential assignment of insoluble proteins of small size, without any specific deuteration requirement. By combining two three-dimensional $^{1}$H detected experiments correlating a $^{13}$C DQ dimension respectively to its intra-residue and sequential $^{15}$N-$^{1}$H pairs, a sequential walk through DQ (Cα+CO) resonance is obtained. Our approach takes advantage of fast MAS to achieve an efficient sensitivity and the addition of a DQ dimension provides spectral features useful for the resonance assignment process.

## Introduction

Solid-state nuclear magnetic resonance spectroscopy (SSNMR) is a powerful technique to study insoluble, aggregated or non-crystalline biomaterials, ranging from biopolymers ((Kelly et al. 2020), (Zhao et al. 2020),(Goldberga et al. 2018)), carbohydrates ((El Hariri El Nokab and van der Wel 2020)), RNA (Ahmed et al. 2020) or membranes (Dufourc 2021),(Mallikarjunaiah et al. 2019) to larger systems such as protein complexes(Demers et al. 2018) large proteins (Vasa et al. 2018)(Schütz 2021)), protein-

ligand interaction ((Vasa et al. 2019)(Elkins and Hong 2019),(Medeiros-Silva et al. 2019)), misfolded proteins (König et al. 2019), amyloid (Tycko 2016)fibrils ((Jaroniec 2019),(Loquet et al. 2018)), helical filaments (Habenstein et al. 2019), viruses (Lecoq et al. 2020), (Gupta et al. 2020), (Lu et al. 2020)), membrane proteins (McDermott 2009)(Tang et al. 2013)(Mandala et al. 2018) or whole cells ((Narasimhan et al. 2020)). In the two past decades, structural investigation of biomolecules at atomic resolution by SSNMR has made dramatic analytical improvements with the introduction of direct proton ($^{1}$H) detection(Ishii et al. 2001)(Reif et al. 2001)(Paulson et al. 2003)(Zhou et al. 2009) combined with the use of magic-angle spinning (MAS) probes operating at fast frequencies(Nishiyama 2016)(Böckmann et al. 2015)(Cala-De Paepe et al. 2017)(Sternberg et al. 2018)(Xue et al. 2018)(Ishii et al. 2018)(Schledorn et al. 2020), nowadays commercially available at MAS frequency of 60-110 kHz. $^{1}$H-detection takes advantage of the high gyromagnetic ratio of proton spins leading to an excellent sensitivity(Ishii et al. 2001)(Demers et al. 2011), together with the fact that $^{1}$H are highly abundant in biomolecules. Fast MAS probes require sub-milligram sample quantities, and well-resolved 3D and 4D $^{1}$H-detected experiments of deuterated ((Knight et al. 2011)(Agarwal et al. 2014)(Fricke et al. 2017)) and fully protonated proteins ((Stanek et al. 2016)(Andreas et al. 2016)(Xiang et al. 2015)(Vasa et al. 2019) have been obtained for protein samples.

Two-dimensional (2D) $^{1}$H-detected correlation experiments such as 2D $^{13}$C-$^{1}$H spectra offer a powerful spectroscopic tool to monitor chemical shift perturbations. These spectral "fingerprints" have the potential to become the new routine experiment for SSNMR investigations of proteins, in analogy to the $^{15}$N-$^{1}$H HSQC experiment for solution NMR, as we recently demonstrated to rapidly compare amyloid fibril conformation of various α-synuclein fibril polymorphs based on 2D $^{15}$N/$^{13}$C-$^{1}$H spectra (De Giorgi et al. 2020). Although few minutes to hours are required to obtain these spectral fingerprints, a tremendous time is still required to perform the so-called resonance assignment step, usually based on 3D experiments to establish triple resonance connectivity's between $^{1}$H, $^{13}$C and $^{15}$N atoms(Barbet-Massin et al. 2014)(Penzel et al. 2015)(Fricke et al. 2017). The assignment process relies on two main steps: first the identification of intra-residue signals including backbone and side chain atoms, and then the establishment of one or more sequential connectivity's between two adjacent residues in the sequence. These sequential assignment experiments have been designed to sequentially link intra (*i*) and proceeding (*i-1*) Cα, CO and Cβ nuclei in correlation with their $^{15}$N and $^{1}$H$^{N}$ backbone nuclei. The efficiency of these

experiments(Barbet-Massin et al. 2014) typically relies on the MAS frequency, the protonation level and the structural homogeneity of the samples. For protonated samples at 100 kHz MAS, the backbone assignment can be extended with the set of 6 Hα-detected experiments(Stanek et al. 2016). The combination of both amide $H^N$ and CαHα-detected experiments can significantly simplify the sequential assignment procedure(Wiegand et al. 2020)(Schubeis et al. 2020), even more by using $H^N$ / CαHα simultaneous acquisition (Sharma et al. 2020)(Stanek et al. 2020) as recently developed for automatic resonance assignment.

Several spectroscopic and biochemistry solutions have been developed to overcome the resonance assignment process, such as the use of higher spectral dimensionality (>3), however, it requires more experimental time in order to achieve a sufficient signal-to-noise ratio (SNR)(Xiang et al. 2014)(Fraga et al. 2017)(Zinke et al. 2017). Another solution is the use of non-uniform isotope labeling strategies to reduce the number of $^{1}H$ and $^{13}C$ sites, such as sparse(Higman et al. 2009), selective(Hoffmann et al. 2018) and segmental labeling schemes(Skrisovska et al. 2010). These methods can reduce the number of overlapping peaks, however additional steps of sample preparation are required, associated with extra costs.

The uniqueness of $^{13}C$ resonances (e.g. Cα of Gly, Cβ for Ala, Thr and Ser) offers one of the most valuable starting point for the identification of the residue-type, and another spectroscopic option to help the resonance assignment process is to decrease the peak overlap via the acquisition of the $^{13}C$ dimension in the double-quantum (DQ) mode. To overcome peak overlapping, a better spectral dispersion can be created from the summation of different spectral regions, ideally in protein samples with Cα+Cβ and Cα+CO. Addition of a DQ dimension helps to increase the spectral dispersion of otherwise overlapping peaks(Luca and Baldus 2002)(Koźmiński and Zhukov 2004) in protein NMR spectra. The DQ dimension is achieved when the magnetization is excited and then back recovered to a zero quantum (SQ) mode using recoupling schemes. This approach has been implemented for dipolar- and scalar-based 2D(Lesage et al. 1997)(Hong 1999) and 3D spectra INADEQUATE-type experiments have been used to simplify the analysis of $^{13}C$-$^{13}C$ correlations(Luca and Baldus 2002)(Chordia et al. 2021). Li *et al*(Li et al. 2020) recently reported the detection of DQ-SQ correlations with a $^{13}C$ detection to increase the spectral resolution of side-chain carboxyl groups of Glu, Asp, Gln and Asn residues. Xiao et al (Xiao et al. 2021) applied Cα-Cβ DQ filtering for Ala, Thr and Ser residues to simplify the 2D and 3D $^{15}N$-$^{13}C$-$^{13}CX$ experiments.

We (Tolchard et al. 2018) and others(Ward et al. 2011) took advantage of direct $^{1}$H detection to generate a $^{13}$C DQ dimension leading to an efficient polarization transfer for correlating $^{13}$C to $^{1}$H spins in protein samples. In 2011, Ladizhansky and coworkers reported the use of 3D DQ(CXCa)NH and DQ(CaCO)NH experiments at moderate MAS frequency (28 kHz) using a SPC-5 sequence on a deuterated membrane protein sample to help the backbone assignment process(Ward et al. 2011). In 2018 we demonstrated, in the case of a fully protonated protein amyloid fibril sample, that a 3D DQ(CXCY)CYH correlation experiment at 70 kHz MAS can provide an efficient strategy to detect side-chains $^{1}$H and $^{13}$C resonances (Tolchard et al. 2018). Because a single 3D experiment was developed in this previous study, the work only permitted a signal identification without the possibility to perform sequential assignment.

In the following, we demonstrate the complete sequential resonance assignment of a medium-size protein assembly through the use of two DQ experiments to access intra-residue and sequential correlations, without a specific deuteration requirement. We take advantage of several spectroscopic features obtained at fast MAS (70 kHz) combined with the use of $^{1}$H-detection to implement high sensitivity 3D correlation experiments using a $^{13}$C DQ dimension. Combination of DQ($Ca_iCX_i$)$N_iH_i$ and DQ($CO_{i-1}Ca_{i-1}$)$N_iH_i$ experiments, complemented by a simple 3D CαNH, leads to a straightforward assignment process based on sequential (Cα+CO) plans. Our approach is demonstrated with the assignment of the amyloid fibrils HET-s in its fully protonated form.

## Materials and methods

### Sample preparation

$^{13}$C/$^{15}$N-labeled, fully protonated HET-s(218-289) was expressed in E. coli, purified and aggregated based on previously described protocols (Balguerie et al. 2003). Approximately 800 µg of HET-s(218-289) amyloid fibrils were introduced in a 1 mm JEOL SSNMR rotor. The tripeptide N-formyl-L-Met-L-Leu-L-Phe (fMLF) was purchased from CortecNet and packed into a 1 mm JEOL ssNMR rotor.

### Solid-state NMR spectroscopy

All spectra were recorded with a 21.1 T (900 MHz $^{1}$H Larmor frequency) JEOL spectrometer equipped with a 1 mm triple resonance HCN MAS probe. The sample temperature was kept at 290 K and the MAS frequency set to 70 kHz. For the BaBa excitation and recovery, we used 1.33 µs long pulses at 188 kHz for total of 457 µs. The detailed spectral acquisition and processing parameters are provided in **Tables S2** and **S3**.

The spectra were processed using JEOL Delta and NMRPipe (Delaglio et al. 1995) software and analyzed using CcpNmr program (Vranken et al. 2005).

## Results and discussion

### Pulse sequence design

Inspired by the work of Ladizhansky (Ward et al. 2011) and our work (Tolchard et al. 2018), we propose two 3D SSNMR MAS experiments (the overall sequence shown in **Fig.1A.**) using DQ excitation and recovery using the back-to-back (BaBa)-xy16 recoupling(Sommer et al. 1995) (Feike et al. 1996), considering that such recoupling is efficient at fast (>60 kHz) MAS regime(Saalwächter et al. 2011)(Tolchard et al. 2018). Moreover, the broadband performance of the BaBa coupling is proportional to the MAS frequency, making it particularly attractive under high $B_0$ field at faster spinning frequencies. It is also robust to radio-frequency field inhomogeneity(Saalwächter et al. 2011) and provides high DQ filtering efficiency. During the BaBa recoupling the magnetization is transferred only between spatially proximate $^{13}C$ spins via dipolar couplings due to dipolar truncation, since recoupled DQ Hamiltonians do not commute each other. Thus, the transfer will preferentially occur between covalently coupled $^{13}C$ spins, making the BaBa recoupling a highly selective way to achieve polarization transfer between two carbon sites within the same residue. We implemented BaBa recoupling in (i) a DQ($Ca_iCX_i$)$N_iH_i$ sequence, which is detecting the $^{13}C$ DQ dimension as the sum of (Cα+Cβ) and (Cα+CO) of intra residue and (ii) a DQ($CO_{i-1}Ca_{i-1}$)$N_iH_i$, experiment which displays the sum of (Cα+CO) of the proceeding residue.

The overall structure for the DQ($Ca_iCX_i$)$N_iH_i$ and DQ($CO_{i-1}Ca_{i-1}$)$N_iH_i$ 3D SSNMR pulse sequences with schematic magnetization pathways are shown in **Fig.1B**. Both sequences start with a cross-polarization (CP) transfer from $^1H$ spins to either Cα or CO spins, depending on the placement of the frequency carrier, to provide a frequency-selective polarization on Cα and CO for the DQ($Ca_iCX_i$)$N_iH_i$ and DQ($CO_{i-1}Ca_{i-1}$)$N_iH_i$ experiments respectively. The following 90$^o$ pulse is applied to create the longitudinal magnetization. The DQ coherence for the first dimension detection (t1) is generated using a BaBa-XY16 excitation(Saalwächter et al. 2011). During this period, the signal can be acquired as the sum of (C+C) resonances, following two polarization patterns. In the DQ($Ca_iCX_i$)$N_iH_i$ experiment, a DQ($C\alpha_iCX_i$) is generated to access the sum of Cα to both carbonyl (CO) and Cβ nuclei, in order to probe the intra-residue spin system. In the DQ($CO_{i-1}Ca_{i-1}$)$N_iH_i$

experiment, a DQ(COCα) is generated to provide the sum of CO to the adjacent Cα. The reconversion is achieved through another block of BaBa recoupling. The 10 kHz CW $^{1}$H decoupling was applied during each BaBa 90$^{o}$ pulse and t1 and t2 acquisition periods. The subsequent $^{13}$C 90$^{o}$ pulse sets the magnetization back to transverse plane and it is transferred to $^{15}$N spins through a $^{13}$C-$^{15}$N CP step, followed by the second dimension detection (t2). The next $^{15}$N 90$^{o}$ pulse sets the magnetization along longitudinal plane for the MISSISIPPI(Zhou and Rienstra 2008) water suppression and another 90$^{o}$ $^{15}$N pulse transfers the magnetization back to the transverse plane. In the last step, a $^{15}$N-$^{1}$H CP step is applied to transfer the magnetization back to $^{1}$H spins for the direct detection (t3), applying a WALTZ16 decoupling for $^{15}$N spins. The overall transfer steps can be written as $H \xrightarrow{CP} C\alpha_i \xrightarrow{BaBa} DQ(C\alpha + C\beta/CO)_i(t_1) \xrightarrow{CP} N_i(t_2) \xrightarrow{CP} NH_i(t_3)$ for 3D DQ($Ca_iCX_i$)$N_iH_i$ and as $H \xrightarrow{CP} CO_{i-1} \xrightarrow{BaBa} DQ(C\alpha + CO)_{i-1}(t1) \xrightarrow{CP} N_i(t_2) \xrightarrow{CP} NH_i(t_3)$ for 3D DQ($CO_{i-1}Ca_{i-1}$)$N_iH_i$ experiments. To obtain a selective polarization transfer to the adjacent carbon, a short mixing was chosen (229 μs) during the BaBa excitation. In this way, a selective DQ coherence is created to correlate $C\alpha_i$ to its neighboring $C\beta_i$ and $CO_i$ spins in the DQ($Ca_iCX_i$)$N_iH_i$ experiment. In the DQ($CO_{i-1}Ca_{i-1}$)$N_iH_i$ experiment, the carbonyl $CO_{i-1}$ has only one neighboring carbon (i.e. $C\alpha_{i-1}$). Both sequences were implemented in the same way, with only difference being the position of the frequency carrier for the first $^{1}$H-$^{13}$C and second $^{13}$C-$^{15}$N CP transfer. Hence the optimized condition can be conveniently transferred between two sequences.

**Polarization transfer efficiency at fast MAS**

In order to estimate the polarization transfer efficiency of BaBa recoupling under 70 kHz MAS, we compared 1D $^{1}$H spectra after a ($^{1}$H-Cα)-$^{1}$H and a ($^{1}$H-Cα-BaBa-Cα)-$^{1}$H polarization pathway respectively. We used the fully protonated protein HET-s(218-289) as a protein benchmark. HET-s(218-289) forms amyloid fibrils, this sample was already used by our laboratory to test pulse sequences at fast MAS regime(Stanek et al. 2016)(Tolchard et al. 2018). From the overlay of spectra showed in **Fig.S1,** we determine that the DQ filter yields to 40% of intensity compared to the pulse sequence employing only CP transfers. This result is comparable to values obtained for other SSNMR homonuclear recoupling sequences (De Pape 2012).

Next, we acquired 1D $^{1}$H spectra to evaluate the transfer efficiencies of DQ($Ca_iCX_i$)$N_iH_i$ and DQ($Ca_iCX_i$)$N_iH_i$ experiments for the fully protonated fMLF sample and HET-s(218-289) amyloid fibrils. We compared the two DQ-based sequence to well-

established hCaNH, hCONH hcoCacoNH, hCOcaNH and hcaCbcaNH experiments (described in details in (Barbet-Massin et al. 2014). To set up a reference for intensity comparison, we used a 1D hNH experiment. This experiment uses only two CP steps and was used before as the standard for the comparison of $^{1}$H detected spectra(Barbet-Massin et al. 2014)(Andreas et al. 2015)(Xiang et al. 2015)(Vallet et al. 2020). The relative intensities of all experiments to the hNH experiment are summarized in **Table S1**. DQ($Ca_iCX_i$)$N_iH_i$ and DQ($Ca_iCX_i$)$N_iH_i$ experiments compared to hCaNH, hCOcaNH, hcaCbcaNH and hCONH experiment are summarized in **Table 1**. Each spectrum was adjusted based on the number of scans. As already observed for deuterated samples(Barbet-Massin et al. 2014)(Xiang et al. 2015)(Penzel et al. 2015) the highest intensities is observed for the hCaNH experiment, leading to ~0.17 transfer efficiency compared to the hNH experiment for the fMLF sample. For deuterated back-exchanged protein samples at 40-60 kHz MAS, these values were higher, i.e. ~0.20-0.30 for hCaNH (Barbet-Massin et al. 2014)(Fricke et al. 2017)(Vallet et al. 2020). These differences can be attributed to longer $^{13}$C and $^{1}$H $T_{1\rho}$ relaxation times for deuterated samples, leading to more efficient transfers and a higher proton sensitivity. Here, the use of the DQ filter leads to a remarkable polarization transfer efficiency compared to the well-established SQ experiments (**Table 1**), demonstrating the benefit of adding the BaBa excitation and reconversion recoupling schemes. The overall DQ($Ca_iCX_i$)$N_iH_i$ and DQ($CO_{i-1}Ca_{i-1}$)$N_iH_i$ experiments lead to a transfer efficiency of ~1.4-5% compared to the hNH experiment for both samples (**Table S1**). The DQ($Ca_iCX_i$)$N_iH_i$ transfer efficiency to correlate intra-residue spins is ~0.31 compared to the hCaNH experiment for the fMLF sample. A similar result (~0.37) is obtained for HET-s(218-289) amyloid fibrils (**Table 1**). For the DQ experiment correlating $CO_{i-1}$ spins to its sequential $N_iH_i$ pair, a polarization transfer efficiency compared to the hCONH experiment of 0.16 and 0.19 was measured for fMLF and HET-s(218-289) samples respectively (**Table 1**). For inter-residual Ca correlation DQ($CO_{i-1}Ca_{i-1}$)$N_iH_i$ experiment is 0.25 and 0.44 less intensive compare to the hcoCacoNH sequence. The efficiency of the DQ($Ca_iCX_i$)$N_iH_i$ to detect intra-residue CO is higher to the hCOcaNH sequence (**Table S1**), which is important experiment for sequential assignment, but is one of the least efficient of 3D assignment experiments (Barbet-Massin et al. 2014)(Penzel et al. 2015). Thus, obtaining intra-residue CO chemical shift with a higher sensitivity is additional advantage for DQ($Ca_iCX_i$)$N_iH_i$ sequence over INEPT based experiment. To estimate the efficiency of the DQ($Ca_iCX_i$)$N_iH_i$ sequence to provide a polarization transfer to intra-residue Cβ spins, we compared to the hcaCbcaNH sequence, which has been reported as one of the

most sensitive sequence to detect Cβ spins(Penzel et al. 2015). The relative intensity of the hcaCbcaNH experiment was ~1% compared to a hNH experiment for HET-s(218-289) fibrils (~3% for fMLF). A relative intensity of ~5% for fMLF and HET-s(218-289) was obtained for the DQ($C\alpha_iCX_i$)$N_iH_i$ sequence (**Table S1**). These values obtained here for protonated systems are lower to reported values obtained for deuterated proteins (6%-16%)(Barbet-Massin et al. 2014)(Penzel et al. 2015)(Vallet et al. 2020), due to the shorter $T_2'$ transverse relaxation times for protonated sample. The lower absolute sensitivity for hCOcaNH and hcaCbcaNH experiments is attributed to the relatively poor sensitivity of scalar-based CC transfers with multiple echo delays. However, this drawback is compensated by a more selective polarization transfer, as hCOcaNH and hcaCbcaNH are optimized to selectively target CO and Cβ spins respectively, while in DQ-based experiments a broader polarization transfer is obtained.

**Table 1**. Relative intensity of 1D experiments recorded on fMLF and HET-s(218-289) amyloid fibrils at 70 kHz MAS.

| Experiment comparison | Relative intensity | |
|---|---|---|
| | **fMLF** | **HET-s(218-289)** |
| DQ($Ca_iCX_i$)$N_iH_i$ / hCaNH | 0.31 | 0.37 |
| DQ($CO_{i-1}Ca_{i-1}$)$N_iH_i$ / hCONH | 0.16 | 0.19 |
| DQ($Ca_iCX_i$)$N_iH_i$ / hCOcaNH | 4.2 | 3 |
| DQ($CO_{i-1}Ca_{i-1}$)$N_iH_i$ / hcoCacoNH | 0.25 | 0.44 |
| DQ($Ca_iCX_i$)$N_iH_i$ / hcaCbcaNH | 1.7 | 4.8 |

**Protein resonance assignment strategy using $^{13}$C DQ-detected experiments**

The resonance assignment strategy relies on the establishment of connectivities between intra-residue pairs (Cα-CO and Cα-Cβ) to their NH pair and between the (Cα-CO) pair to its sequential NH pair. To disentangle the SQ Cα chemical shift to the signal provided by the (Cα+Cβ) and (Cα+CO) DQ resonances, a single 3D hCaNH experiment is additionally required. In the 3D DQ($Ca_iCX_i$)$N_iH_i$ spectrum, each individual NH strip displays the sum of intra-residue (Cα+Cβ) and (Cα+CO) resonances. The Cβ(*i*) and CO(*i*) shifts can be calculated by subtracting Cα (*i*) shifts (acquired in hCaNH spectrum) from the additions of (Cα+Cβ) or (Cα+CO) DQ resonances. In this manner we can obtain the Cα, Cβ and CO triplet for the same residue. Then the 3D DQ($CO_{i-1}Ca_{i-1}$)$N_iH_i$ experiment provides the sum of

(Cα+CO) resonance of the proceeding *i-1* residue and is matched to the sum of (Cα+CO) of intra-residue resonance. As a consequence, the difference of ($C\alpha_i$+$CO_i$) and ($C\alpha_i$+$CO_i$) resonances will result in a single $C\alpha_{i-1}$ shift. In such manner, a sequential backbone walk is achieved by employing only three 3D experiments, which then give access to intra-residue H, N, Cα, Cβ and CO as well as Cα and CO chemical shifts of the proceeding residue.

**Completeness of the assignment strategy**

For the fMLF tripeptide, we assign all anticipated intra-residue and sequential correlations in the two 3D DQ-detected spectra (the 2D $^{1}H$-$^{13}C$ strips from 3D spectra are shown in **Fig.2A**). The assignment was confirmed with comparison of previously published chemical shifts for the fMLF peptide(Struppe et al. 2017). For the Cβ assignments in 2D strips of hcaCbcaNH spectrum we found 2 out for 3 expected peaks. The absence of Cβ peak for the Leu residue (**Fig.2A**), might be attributed to ongoing dynamics at different time scale, which can hinder the scalar coupling-based magnetization transfer. Leu Cβ spin is detected in the 3D DQ($Ca_iCX_i$)$N_iH_i$ spectrum. Due to even lower sensitivity of 1D hcaCbcaNH experiment for HET-s(218-289) we didn't acquired as 3D spectrum. For HET-s(218-289) the Cβ shifts were obtained solely from the DQ($Ca_iCX_i$)$N_iH_i$ spectrum by subtraction of Cα shifts from the sum of (Cα+Cβ) peaks.

Both DQ($Ca_iCX_i$)$N_iH_i$ and DQ($CO_{i-1}Ca_{i-1}$)$N_iH_i$ experiments also provide a larger $^{13}C$ connection maps compare to SQ $^{13}C$ dimension experiments. The sequential backbone walk using $^{13}C$ DQ experiments were conducted through 2D $^{1}H$-$^{13}C$ projections along $^{15}N$ dimension of 3D DQ($Ca_iCX_i$)$N_iH_i$ and DQ($CO_{i-1}C\alpha_{i-1}$)$N_iH_i$ spectra in a combination with 3D hCaNH spectrum (**Fig.2B**). We use the 3D DQ($Ca_iCX_i$)$N_iH_i$ spectrum to access (Cα+Cβ) and (Cα+CO) intra-residue correlations. In the 3D DQ($CO_{i-1}C\alpha_{i-1}$)$N_iH_i$ experiment, the sum (Cα+CO) of *i-1* peaks (blue peaks in **Fig.2B**) can be directly connected to (Cα+CO) of *i* residue (green peaks in **Fig.2B**). Interestingly, we noticed additional weak intensity peaks in 2D planes of 3D DQ($Ca_iCX_i$)$N_iH_i$. These peaks perfectly matched the sum (Cα+Cβ) of the proceeding residue. Similar observation based on the observation of weak *i-1* correlations has been described for solution NMR HNCa experiment(Kay et al. 1990). The origins of these unexpected peaks might be due to non-selective band excitation of BaBa recoupling (**Fig.2B**). As a consequence, the DQ coherence can spread to weakly coupled carbons through dipolar couplings. On one side, these additional peaks are reducing the peak intensities of intra-residue correlations due to dipolar truncation. On the other side, they

provide additional information to establish a sequential link. Overall the DQ($Ca_iCX_i$)$N_iH_i$ and DQ($CO_{i-1}Ca_{i-1}$)$N_iH_i$ spectra showed expected intra-residue and sequential correlation for the fMLF peptide.

Next, we demonstrated the approach on a medium-size insoluble protein assembly, the amyloid fibrils of HET-s(218-289). At 70 kHz MAS, we measured a $^1$H line-width of ~250 Hz on a 21 Tesla magnet (900 MHz $^1$H Larmor frequency) from a 2D hNH spectrum (**Fig.S2**). Such a $^1$H line-width is close to the value reported for the same fibrillar protein system acquired at 100 kHz MAS (at 1 GHz $^1$H Larmor frequency) (Stanek et al. 2016). We observed slightly lower signal intensities (compare to hNH) for 3D INEPT-based assignment experiments for HET-s(218-289) amyloid fibrils compared to the fMLF sample, due to additional relaxation effects that lead to less efficient polarization transfers. However, the overall intensity for the DQ($Ca_iCX_i$)$N_iH_i$ experiment was comparable to fMLF and it was even higher for the DQ($CO_{i-1}Ca_{i-1}$)$N_iH_i$ experiment. It might indicate that both $^{13}$C DQ-based experiments are more prone to slower transverse relaxation times as present for the HET-s sample. An overlay of 2D DQ-$^{13}$C/$^{15}$N projections for 3D DQ($Ca_iCX_i$)$N_iH_i$ and hCaNH experiments (**Fig.3A**) and DQ($CO_{i-1}Ca_{i-1}$)$N_iH_i$ and hCONH experiments (**Fig.3B**). All cross-peaks in the 3D DQ-detected experiments are well spread out, and the inclusion of the Cβ resonances does not increase the spectral overlap since it is encoded via a DQ dimension. As a consequence, most (Cα+Cβ) resonances are spread around 85-130 ppm, and do not overlap with Cα signals (45-65 ppm). The lowest sum of (Cα+Cβ) peaks arise from Ala residues, hence they are shifted in the upfield part of the spectrum, around 70 ppm (**Fig.3A**). Gly residues, due to the absence of a Cβ atom, appear only as the sum of (Cα+CO) peaks (**Fig.3B**) shifted upfield (~ 45 ppm) compare to other DQ resonances. As expected, the most downfield shifted signals in (Cα+Cβ) region belong to Thr and Ser residues, due to their higher chemical shift values. All other residues have DQ resonances that appear in between the sum of (Cα+Cβ) resonances of Thr/Ser and Ala residues. We notice that for several aliphatic residues, resonances overlap in the hCaNH spectrum (red spectrum in **Fig.3A**), for instance residues 267V, 231I and 229K. This can cause additional ambiguities for the protein chemical shift assignment. In the DQ($Ca_iCX_i$)$N_iH_i$ spectrum (green spectrum in **Fig.3A**) the DQ-detected resonance for the same residues were more clearly dispersed due to generated sum of (Cα+Cβ) resonance in the DQ $^{13}$C dimension. This spectral feature of DQ $^{13}$C-detected experiments provides a similar advantage for the detection of $CO_{i-1}$ resonances in DQ($CO_{i-1}Ca_{i-1}$)$N_iH_i$ compared to hCONH experiment (spectral overlay is shown in **Fig.3B**).

We employed a similar strategy, as previously described for the fMLF peptide, to carry out the sequential assignment of HET-s(218-289) resonances. The resonance assignment strategy on a protein sample is illustrated in **Fig.3C**. The 2D $^{1}$H-DQ$^{13}$C strip plots along $^{15}$N dimension are particularly efficient to provide a sequential protein backbone assignment using combination of 3D DQ($Ca_iCX_i$)$N_iH_i$, DQ($CO_{i-1}Ca_{i-1}$)$N_iH_i$ and hCaNH experiments. Using this approach, we achieve the assignment of 87.5 % of backbone HN, 81.2 % of intra-residue $^{13}$C and we establish a sequential connectivity for 87.5% of the residues in the rigid core of HET-s(218-289) amyloid fibrils.

One advantage of the DQ-based sequential backbone assignment is the requirement of a set of only three 3D experiments. The two 3D experiments (DQ($Ca_iCX_i$)$N_iH_i$ and DQ($CO_{i-1}Ca_{i-1}$)$N_iH_i$) were recorded in 5 days and provided enough sensitivity and spectral dispersion to perform a *de novo* assignment (in combination with a hCaNH, which took 15 h to acquired) of fully protonated HET-s(218-289) amyloid fibrils. The combination of both 3D DQ($Ca_iCX_i$)$N_iH_i$ and DQ($CO_{i-1}Ca_{i-1}$)$N_iH_i$ spectra with hCaNH allows to identify backbone chemical shifts, to link sequential Cα-CO pairs and to detect intra-residue Cβ spins. Additionally, the approach artificially increases the $^{13}$C signal dispersion for otherwise overlapping peaks due to the DQ dimension. In order to cover the large chemical shift differences in the DQ $^{13}$C dimension, both DQ($Ca_iCX_i$)$N_iH_i$ and DQ($CO_{i-1}Ca_{i-1}$)$N_iH_i$ experiments need however to be acquired with a sufficiently large sampling rates in the indirect DQ $^{13}$C dimension (details shown in **Tables S2** and **S3**). In that regard, the number of scans for an adequate measurement time must be leveraged in order to achieve high enough SNR.

Completeness of the HET-s(218-289) resonance assignment using the DQ-detected approach was determined to be ~87 % of $^{13}$C, $^{15}$N and $^{1}$H resonances, considering the rigid residues of the amyloid core observable in a CP experiment. This result is comparable to previously reported resonance assignment strategies on the same protein using conventional $^{13}$C-detected (Siemer et al. 2006b)(Van Melckebeke et al. 2010) and $^{1}$H-detected SSNMR experiments (Smith et al. 2017) (Tolchard et al. 2018) (Stanek et al. 2016). The missing residues in $^{1}$H detected spectra have been reported for other proteins(Torosyan et al. 2019)(Jirasko et al. 2021). We hypothesize that these atoms are involved in a faster dynamic range that averages out dipole couplings and therefore weakens the CP transfer step. The access to these residues would be possible using INEPT or direct polarization during the first

magnetization initiation step as demonstrated by Meier and coworkers(Lange et al. 2011)(Siemer et al. 2006a)(Siemer 2020).

## Conclusions

In this study, we demonstrate the potential of introducing a $^{13}$C DQ dimension in 3D SSNMR $^{1}$H-detected experiments at fast MAS to perform protein resonance assignment. The use of a $^{13}$C DQ dimension using the Baba recoupling provides a remarkable sensitivity to achieve $^{13}$C-$^{13}$C polarization transfer at fast MAS (70 kHz) and increases the $^{13}$C spectral dispersion. The approach was demonstrated on fully protonated HET-s fibrils to access the detection of $^{13}$C, $^{15}$N and $^{1}$H backbone spins, detect intra-residue Cβ, Cα, CO and sequentially link Cα-CO pairs. For small-to-medium size proteins typically studied by SSNMR (i.e. ~30-100 amino-acids detected in a CP experiment), the approach is a promising alternative to conventional out-and-back techniques using CC scalar transfers popularized by Pintacuda and coworkers(Barbet-Massin et al. 2013)(Barbet-Massin et al. 2014). The ever-increasing faster MAS frequencies in combination with higher magnetic fields will be also beneficial for DQ-based sequences, due to increased broadband range for the BaBa recoupling and longer $^{13}$C and $^{1}$H $T'_2$ relaxation times. Further on, we are going to expand $^{13}$C DQ sequences to combine them with Hα detection methods and implement them into automatic assignment programs.

## Acknowledgments

We acknowledge financial support from the European Research Council (ERC) under the European Unions Horizon 2020 research and innovation program (ERC-2015-StG GA no. 639020 to A. Loquet). The project was supported by FranceAgriMer and the CNIV through the program PNDV (project ATOMIVINE n° 297772) and the IdEx Bordeaux (Chaire d'Installation to B.H., ANR-10-IDEX-03-02). A. Lends was supported by the Swiss National Science Foundation for early postdoc mobility project P2EZP2_184258. This work was supported by JSPS KAKENHI Grant Number 20K05483 and in part by the JST-Mirai Program (Grant No. JPMJMI17A2, Japan) to Y. Nishiyama.

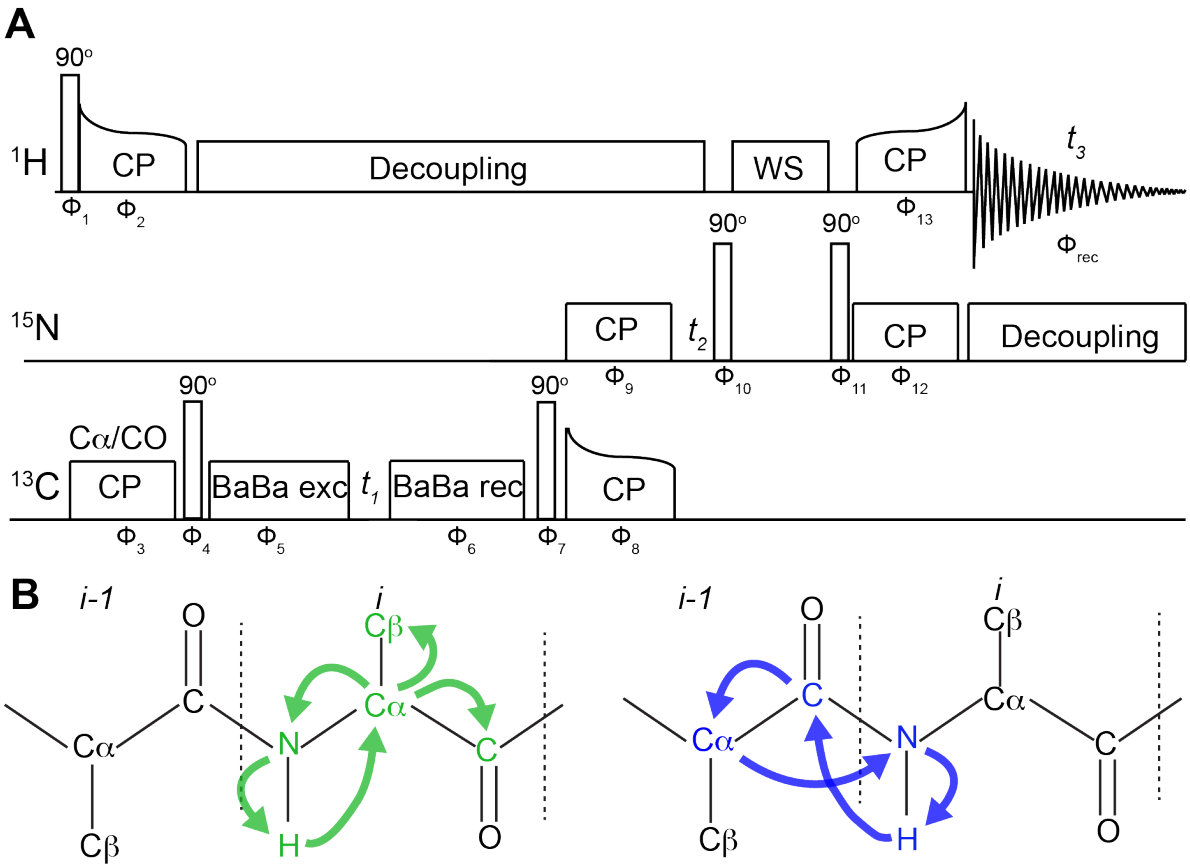


**Fig.1. A** Pulse sequence of the 3D DQ($Ca_iCX_i$)$N_iH_i$, DQ($CO_{i-1}Ca_{i-1}$)$N_iH_i$ experiments. The initiation of corresponding polarization transfers are achieved through the carrier value of the first $^{1}$H-$^{13}$C cross-polarization transfer. The applied phase cycling was executed with the following scheme $\Phi_1$={8(x), 8(-x)}, $\Phi_2$={x},$\Phi_3$={x}, $\Phi_4$={-x}, $\Phi_5$={x,-x,y,-y}, $\Phi_6$={x}, $\Phi_7$={-x}, $\Phi_8$={x}, $\Phi_9$={4(x), 4(y)},$\Phi_{10}$={x}$\Phi_{11}$={-y}, $\Phi_{12}$={16(x), 16(y)}, $\Phi_{13}$={x}, $\Phi_{rec}$={2(x,y),2(y,x),2(y,x),2(x,y),2(y,x),2(x,y),2(x,y),2(y,x)}. **B** Schematic representation of the polarization transfer pathways and involved spins for DQ($Ca_iCX_i$)$N_iH_i$ (green) and DQ($CO_{i-1}Ca_{i-1}$)$N_iH_i$ (blue) experiments.

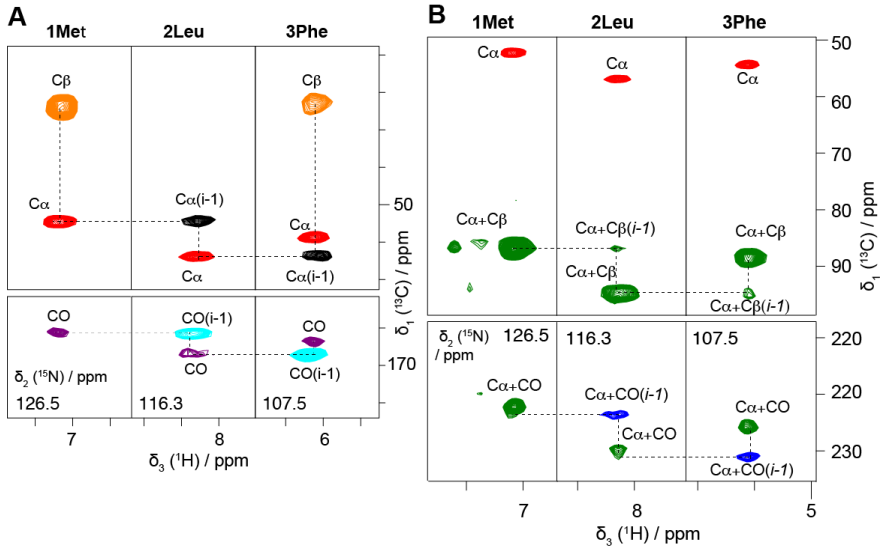


**Fig.2**. 2D projections of $^{1}$H-detected SSNMR experiments recorded on fMLF. **A** the 2D $^{1}$H-$^{13}$C strips along $^{15}$N dimension for the 3D hCaNH (red), hCONH (cyan), hcoCacoNH (black), hcaCbcaNH (orange) and hCOcaNH (purple) spectra. **B** The 2D $^{1}$H-$^{13}$C strips along $^{15}$N dimension for the hCaNH (red), DQ($Ca_iCX_i$)$N_iH_i$ (green) and DQ($CO_{i-1}Ca_{i-1}$)$N_iH_i$ (blue) spectra, the sequential backbone walk is shown with dotted lines.

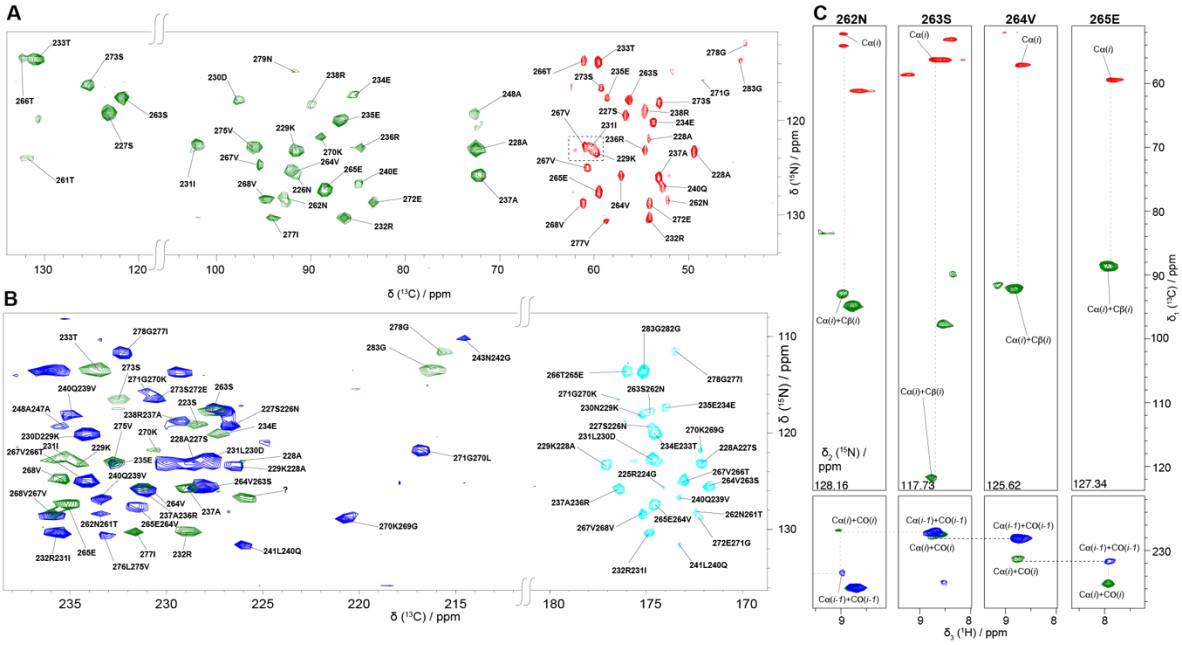


**Fig.3**. 2D projections of $^{1}$H-detected SSNMR experiments recorded on HET-s(218-289) amyloid fibrils. **A** 2D $^{13}$C-$^{15}$N projections of 3D DQ($Ca_iCX_i$)$N_iH_i$ (green) and hCaNH (red) experiments, showing intra-residue Cα, CO, Cα+Cβ and Cα+CO correlations. The overlapping peaks in the N-Cα region is indicated with the dotted square. **B** 2D $^{13}$C-$^{15}$N projections of DQ($CO_{i-1}Ca_{i-1}$)$N_iH_i$ (blue) and hCONH (cyan) experiments, showing the inter

residue CO and Cα+CO regions. **C** 2D $^{1}$H-$^{13}$C strips along $^{15}$N dimension for the sequential backbone walk is shown with dotted lines.

## References

Agarwal V, Penzel S, Szekely K, et al (2014) De novo 3D structure determination from sub-milligram protein samples by solid-state 100 kHz MAS NMR spectroscopy. Angew Chem Int Ed Engl 53:12253–12256. doi: 10.1002/anie.201405730

Ahmed M, Marchanka A, Carlomagno T (2020) Structure of a Protein–RNA Complex by Solid-State NMR Spectroscopy. Angew Chemie - Int Ed 59:6866–6873. doi: 10.1002/anie.201915465

Andreas LB, Jaudzems K, Stanek J, et al (2016) Structure of fully protonated proteins by proton-detected magic-angle spinning NMR. Proc Natl Acad Sci U S A 113:9187–92. doi: 10.1073/pnas.1602248113

Andreas LB, Stanek J, Le Marchand T, et al (2015) Protein residue linking in a single spectrum for magic-angle spinning NMR assignment. J Biomol NMR 62:253–261. doi: 10.1007/s10858-015-9956-1

Balguerie A, Dos Reis S, Ritter C, et al (2003) Domain organization and structure-function relationship of the HET-s prion protein of Podospora anserina. EMBO J 22:2071–2081. doi: 10.1093/emboj/cdg213

Barbet-Massin E, Pell AJ, Jaudzems K, et al (2013) Out-and-back 13C-13C scalar transfers in protein resonance assignment by proton-detected solid-state NMR under ultra-fast MAS. J Biomol NMR 56:379–386. doi: 10.1007/s10858-013-9757-3

Barbet-Massin E, Pell AJ, Retel JS, et al (2014) Rapid proton-detected NMR assignment for proteins with fast magic angle spinning. J Am Chem Soc 136:12489–12497. doi: 10.1021/ja507382j

Böckmann A, Ernst M, Meier BH (2015) Spinning proteins, the faster, the better? J Magn Reson 253:71–79. doi: 10.1016/j.jmr.2015.01.012

Cala-De Paepe D, Stanek J, Jaudzems K, et al (2017) Is protein deuteration beneficial for proton detected solid-state NMR at and above 100 kHz magic-angle spinning? Solid State Nucl Magn Reson 87:126–136. doi: 10.1016/j.ssnmr.2017.07.004

Chordia S, Narasimhan S, Lucini Paioni A, et al (2021) In vivo Assembly of Artificial Metalloenzymes and Application in Whole□Cell Biocatalysis. Angew Chemie Int Ed 2–

10. doi: 10.1002/anie.202014771

De Giorgi F, Laferrière F, Zinghirino F, et al (2020) Novel self-replicating α-synuclein polymorphs that escape ThT monitoring can spontaneously emerge and acutely spread in neurons. Sci Adv 6:. doi: 10.1126/sciadv.abc4364

De Pape G (2012) Dipolar recoupling in magic angle spinning solid-state nuclear magnetic resonance. Annu Rev Phys Chem 63:661–684. doi: 10.1146/annurev-physchem-032511-143726

Delaglio F, Grzesiek S, Vuister GW, et al (1995) NMRPipe: A multidimensional spectral processing system based on UNIX pipes. J Biomol NMR 6:277–293. doi: 10.1007/BF00197809

Demers JP, Chevelkov V, Lange A (2011) Progress in correlation spectroscopy at ultra-fast magic-angle spinning: Basic building blocks and complex experiments for the study of protein structure and dynamics. Solid State Nucl Magn Reson 40:101–113. doi: 10.1016/j.ssnmr.2011.07.002

Demers JP, Fricke P, Shi C, et al (2018) Structure determination of supra-molecular assemblies by solid-state NMR: Practical considerations. Prog Nucl Magn Reson Spectrosc 109:51–78. doi: 10.1016/j.pnmrs.2018.06.002

Dufourc EJ (2021) Bicelles and nanodiscs for biophysical chemistry1. Biochim Biophys Acta - Biomembr 1863:183478. doi: 10.1016/j.bbamem.2020.183478

El Hariri El Nokab M, van der Wel PCA (2020) Use of solid-state NMR spectroscopy for investigating polysaccharide-based hydrogels: A review. Carbohydr Polym 240:116276. doi: 10.1016/j.carbpol.2020.116276

Elkins MR, Hong M (2019) Elucidating ligand-bound structures of membrane proteins using solid-state NMR spectroscopy. Curr Opin Struct Biol 57:103–109. doi: 10.1016/j.sbi.2019.02.002

Feike M, Demco DE, Graf R, et al (1996) Broadband multiple-quantum NMR spectroscopy. J Magn Reson - Ser A 122:214–221. doi: 10.1006/jmra.1996.0197

Fraga H, Arnaud C, Gauto DF, Audin M (2017) Solid-State NMR H – N –( C )– H and H – N – C – C 3D / 4D Correlation Experiments for Resonance Assignment of Large Proteins. 2697–2703. doi: 10.1002/cphc.201700572

Fricke P, Chevelkov V, Zinke M, et al (2017) Backbone assignment of perdeuterated proteins by solid-state NMR using proton detection and ultrafast magic-angle spinning. Nat Protoc 12:764–782. doi: 10.1038/nprot.2016.190

Goldberga I, Li R, Duer MJ (2018) Collagen Structure-Function Relationships from Solid-

State NMR Spectroscopy. Acc Chem Res 51:1621–1629. doi: 10.1021/acs.accounts.8b00092

Gupta S, Louis JM, Tycko R (2020) Effects of an HIV-1 maturation inhibitor on the structure and dynamics of CA-SP1 junction helices in virus-like particles. Proc Natl Acad Sci U S A 117:10286–10293. doi: 10.1073/pnas.1917755117

Habenstein B, Mammeri N El, Tolchard J, et al (2019) Current Topics in Microbiology and Immunology Bacterial Type III Protein Secretion Systems

Higman VA, Flinders J, Hiller M, et al (2009) Assigning large proteins in the solid state: A MAS NMR resonance assignment strategy using selectively and extensively 13C-labelled proteins. J Biomol NMR 44:245–260. doi: 10.1007/s10858-009-9338-7

Hoffmann B, Löhr F, Laguerre A, et al (2018) Protein labeling strategies for liquid-state NMR spectroscopy using cell-free synthesis. Prog Nucl Magn Reson Spectrosc 105:1–22. doi: 10.1016/j.pnmrs.2017.11.004

Hong M (1999) Solid-State Dipolar INADEQUATE NMR Spectroscopy with a Large Double-Quantum Spectral Width. J Magn Reson 91:86–91

Ishii Y, Wickramasinghe A, Matsuda I, et al (2018) Progress in proton-detected solid-state NMR (SSNMR): Super-fast 2D SSNMR collection for nano-mole-scale proteins. J Magn Reson 286:99–109. doi: 10.1016/j.jmr.2017.11.011

Ishii Y, Yesinowski JP, Tycko R (2001) Sensitivity enhancement in solid-state 13C NMR of synthetic polymers and biopolymers by 1H NMR detection with high-speed magic angle spinning. J Am Chem Soc 123:2921–2922. doi: 10.1021/ja015505j

Jaroniec CP (2019) Two decades of progress in structural and dynamic studies of amyloids by solid-state NMR. J Magn Reson 306:42–47. doi: 10.1016/j.jmr.2019.07.015

Jirasko V, Lends A, Lakomek NA, et al (2021) Dimer Organization of Membrane-Associated NS5A of Hepatitis C Virus as Determined by Highly Sensitive 1H-Detected Solid-State NMR. Angew Chemie - Int Ed 60:5339–5347. doi: 10.1002/anie.202013296

Kay LE, Ikura M, Tschudin R, Bax A (1990) Three-dimensional triple-resonance NMR Spectroscopy of isotopically enriched proteins. J Magn Reson 89:496–514. doi: 10.1016/j.jmr.2011.09.004

Kelly JE, Chrissian C, Stark RE (2020) Tailoring NMR experiments for structural characterization of amorphous biological solids: A practical guide. Solid State Nucl Magn Reson 109:101686. doi: 10.1016/j.ssnmr.2020.101686

Knight MJ, Webber AL, Pell AJ, et al (2011) Fast resonance assignment and fold determination of human superoxide dismutase by high-resolution proton-detected solid-

state MAS NMR spectroscopy. Angew Chemie - Int Ed 50:11697–11701. doi: 10.1002/anie.201106340

König A, Schölzel D, Uluca B, et al (2019) Hyperpolarized MAS NMR of unfolded and misfolded proteins. Solid State Nucl Magn Reson 98:1–11. doi: 10.1016/j.ssnmr.2018.12.003

Koźmiński W, Zhukov I (2004) The DQ-HN{CACB} and DQ-HN(CO){CACB} sequences with evolution of double quantum Cα-Cβ coherences. J Magn Reson 171:186–191. doi: 10.1016/j.jmr.2004.08.021

Lange S, Emsley L, Dumez J, Oschkinat H (2011) Spectroscopy of Perdeuterated Proteins under Ultrafast Magic-Angle. 2205–2211

Lecoq L, Fogeron ML, Meier BH, et al (2020) Solid-state NMR for studying the structure and dynamics of viral assemblies. Viruses 12:1–26. doi: 10.3390/v12101069

Lesage A, Auger C, Caldarelli S, Emsley L (1997) Determination of through-bond carbon-carbon connectivities in solid-state NMR using the INADEAUATE experiment. J Am Chem Soc 119:7867–7868. doi: 10.1021/ja971089k

Li J, Sae Her A, Traaseth NJ (2020) Site-specific resolution of anionic residues in proteins using solid-state NMR spectroscopy. J Biomol NMR 74:355–363. doi: 10.1007/s10858-020-00323-z

Loquet A, El Mammeri N, Stanek J, et al (2018) 3D structure determination of amyloid fibrils using solid-state NMR spectroscopy. Methods 138–139:26–38. doi: 10.1016/j.ymeth.2018.03.014

Lu M, Russell RW, Bryer AJ, et al (2020) Atomic-resolution structure of HIV-1 capsid tubes by magic-angle spinning NMR. Nat Struct Mol Biol 27:863–869. doi: 10.1038/s41594-020-0489-2

Luca S, Baldus M (2002) Enhanced spectral resolution in immobilized peptides and proteins by combining chemical shift sum and difference spectroscopy. J Magn Reson 159:243–249. doi: 10.1016/S1090-7807(02)00019-8

Mallikarjunaiah KJ, Kinnun JJ, Petrache HI, Brown MF (2019) Flexible lipid nanomaterials studied by NMR spectroscopy. Phys Chem Chem Phys 21:18422–18457. doi: 10.1039/c8cp06179c

Mandala VS, Williams JK, Hong M (2018) Structure and Dynamics of Membrane Proteins from Solid-State NMR. Annu Rev Biophys 47:201–222. doi: org/10.1146/annurev-biophys-070816-033712

McDermott AE (2009) Structure and Dynamics of Membrane Proteins by Magic Angle

Spinning Solid-State NMR. Annu Rev Biophys 38:385–403. doi: 10.1146/annurev.biophys.050708.133719

Medeiros-Silva J, Jekhmane S, Breukink E, Weingarth M (2019) Towards the Native Binding Modes of Antibiotics that Target Lipid II. ChemBioChem 20:1731–1738. doi: 10.1002/cbic.201800796

Narasimhan S, Folkers GE, Baldus M (2020) When Small becomes Too Big: Expanding the Use of In-Cell Solid-State NMR Spectroscopy. Chempluschem 85:760–768. doi: 10.1002/cplu.202000167

Nishiyama Y (2016) Fast magic-angle sample spinning solid-state NMR at 60–100 kHz for natural abundance samples. Solid State Nucl Magn Reson 78:24–36. doi: 10.1016/j.ssnmr.2016.06.002

Paulson EK, Morcombe CR, Gaponenko V, et al (2003) Sensitive High Resolution Inverse Detection NMR Spectroscopy of Proteins in the Solid State. J Am Chem Soc 125:15831–15836. doi: 10.1021/ja037315+

Penzel S, Smith AA, Agarwal V, et al (2015) Protein resonance assignment at MAS frequencies approaching 100 kHz: A quantitative comparison of J-coupling and dipolar-coupling-based transfer methods. J Biomol NMR 63:165–186. doi: 10.1007/s10858-015-9975-y

Reif B, Jaroniec CP, Rienstra CM, et al (2001) 1H-1H MAS correlation spectroscopy and distance measurements in a deuterated peptide. J Magn Reson 151:320–7. doi: 10.1006/jmre.2001.2354

Saalwächter K, Lange F, Matyjaszewski K, et al (2011) BaBa-xy16: Robust and broadband homonuclear DQ recoupling for applications in rigid and soft solids up to the highest MAS frequencies. J Magn Reson 212:204–215. doi: 10.1016/j.jmr.2011.07.001

Schledorn M, Malär AA, Torosyan A, et al (2020) Protein NMR Spectroscopy at 150 kHz Magic-Angle Spinning Continues To Improve Resolution and Mass Sensitivity. ChemBioChem 21:2540–2548. doi: 10.1002/cbic.202000341

Schubeis T, Le Marchand T, Daday C, et al (2020) A β-barrel for oil transport through lipid membranes: Dynamic NMR structures of AlkL. Proc Natl Acad Sci U S A 117:21014–21021. doi: 10.1073/pnas.2002598117

Schütz AK (2021) Solid-state NMR approaches to investigate large enzymes in complex with substrates and inhibitors. Biochem Soc Trans 49:131–144. doi: 10.1042/BST20200099

Sharma K, Madhu PK, Agarwal V, Mote KR (2020) Simultaneous recording of intra- and inter-residue linking experiments for backbone assignments in proteins at MAS

frequencies higher than 60 kHz. J Biomol NMR 74:229–237. doi: 10.1007/s10858-019-00292-y

Siemer AB (2020) Advances in studying protein disorder with solid-state NMR. Solid State Nucl Magn Reson 106:101643. doi: 10.1016/j.ssnmr.2020.101643

Siemer AB, Arnold AA, Ritter C, et al (2006a) Observation of highly flexible residues in amyloid fibrils of the HET-s prion. J Am Chem Soc 128:13224–13228. doi: 10.1021/ja063639x

Siemer AB, Ritter C, Steinmetz MO, et al (2006b) 13C,15N Resonance assignment of parts of the HET-s prion protein in its amyloid form. J Biomol NMR 34:75–87. doi: 10.1007/s10858-005-5582-7

Skrisovska L, Schubert M, Allain FHT (2010) Recent advances in segmental isotope labeling of proteins: NMR applications to large proteins and glycoproteins. J Biomol NMR 46:51–65. doi: 10.1007/s10858-009-9362-7

Smith AA, Ravotti F, Testori E, et al (2017) Partially-deuterated samples of HET-s(218–289) fibrils: assignment and deuterium isotope effect. J Biomol NMR 67:109–119. doi: 10.1007/s10858-016-0087-0

Sommer W, Gottwald J, Demco DE, Spiess HW (1995) Dipolar Heteronuclear Multiple-Quantum NMR Spectroscopy in Rotating Solids. J. Magn. Reson. Ser. A 113:131–134

Stanek J, Andreas LB, Jaudzems K, et al (2016) NMR Spectroscopic Assignment of Backbone and Side-Chain Protons in Fully Protonated Proteins: Microcrystals, Sedimented Assemblies, and Amyloid Fibrils. Angew Chemie - Int Ed 55:15504–15509. doi: 10.1002/anie.201607084

Stanek J, Schubeis T, Paluch P, et al (2020) Automated Backbone NMR Resonance Assignment of Large Proteins Using Redundant Linking from a Single Simultaneous Acquisition. J Am Chem Soc 142:5793–5799. doi: 10.1021/jacs.0c00251

Sternberg U, Witter R, Kuprov I, et al (2018) 1H line width dependence on MAS speed in solid state NMR – Comparison of experiment and simulation. J Magn Reson 291:32–39. doi: 10.1016/j.jmr.2018.04.003

Struppe J, Quinn CM, Lu M, et al (2017) Expanding the horizons for structural analysis of fully protonated protein assemblies by NMR spectroscopy at MAS frequencies above 100 kHz. Solid State Nucl Magn Reson 87:117–125. doi: 10.1016/j.ssnmr.2017.07.001

Tang M, Comellas G, Rienstra CM (2013) Advanced Solid-State NMR Approaches Proteins and Amyloid Fibrils. Acc Chem Res 46:

Tolchard J, Pandey MK, Berbon M, et al (2018) Detection of side-chain proton resonances of

fully protonated biosolids in nano-litre volumes by magic angle spinning solid-state NMR. J Biomol NMR 70:177–185. doi: 10.1007/s10858-018-0168-3

Torosyan A, Wiegand T, Schledorn M, et al (2019) Including Protons in Solid-State NMR Resonance Assignment and Secondary Structure Analysis: The Example of RNA Polymerase II Subunits Rpo4/7. Front Mol Biosci 6:1–8. doi: 10.3389/fmolb.2019.00100

Tycko R (2016) Molecular structure of aggregated amyloid-β: Insights from solid-state nuclear magnetic resonance. Cold Spring Harb Perspect Med 6:a024083. doi: 10.1101/cshperspect.a024083

Vallet A, Favier A, Brutscher B, Schanda P (2020) ssNMRlib: a comprehensive library and tool box for acquisition of solid-state nuclear magnetic resonance experiments on Bruker spectrometers. Magn Reson 1:331–345. doi: 10.5194/mr-1-331-2020

Van Melckebeke H, Wasmer C, Lange A, et al (2010) Atomic-resolution three-dimensional structure of HET-s(218-289) amyloid fibrils by solid-state nmr spectroscopy. J Am Chem Soc 132:13765–13775. doi: 10.1021/ja104213j

Vasa SK, Singh H, Grohe K, Linser R (2019) Assessment of a Large Enzyme–Drug Complex by Proton-Detected Solid-State NMR Spectroscopy without Deuteration. Angew Chemie - Int Ed 58:5758–5762. doi: 10.1002/anie.201811714

Vasa SK, Singh H, Rovó P, Linser R (2018) Dynamics and Interactions of a 29 kDa Human Enzyme Studied by Solid-State NMR. J Phys Chem Lett 9:1307–1311. doi: 10.1021/acs.jpclett.8b00110

Vranken WF, Boucher W, Stevens TJ, et al (2005) The CCPN data model for NMR spectroscopy: Development of a software pipeline. Proteins Struct Funct Genet 59:687–696. doi: 10.1002/prot.20449

Ward ME, Shi L, Lake E, et al (2011) Proton-detected solid-state NMR reveals intramembrane polar networks in a seven-helical transmembrane protein proteorhodopsin. J Am Chem Soc 133:17434–17443. doi: 10.1021/ja207137h

Wiegand T, Schledorn M, Malär AA, et al (2020) Nucleotide Binding Modes in a Motor Protein Revealed by 31P- and 1H-Detected MAS Solid-State NMR Spectroscopy. ChemBioChem 21:324–330. doi: 10.1002/cbic.201900439

Xiang S, Chevelkov V, Becker S, Lange A (2014) Towards automatic protein backbone assignment using proton-detected 4D solid-state NMR data. J Biomol NMR 60:85–90. doi: 10.1007/s10858-014-9859-6

Xiang SQ, Grohe K, Rovó P, et al (2015) Sequential backbone assignment based on dipolar

amide-to-amide correlation experiments. J Biomol NMR 62:303–311. doi: 10.1007/s10858-015-9945-4

Xiao H, Zhang Z, Zhao Y, Yang J (2021) Spectral editing of alanine , serine , and threonine in uniformly labeled proteins based on frequency  selective homonuclear recoupling in solid  state NMR. J Biomol NMR. doi: 10.1007/s10858-021-00367-9

Xue K, Sarkar R, Motz C, et al (2018) Magic-Angle Spinning Frequencies beyond 300 kHz Are Necessary to Yield Maximum Sensitivity in Selectively Methyl Protonated Protein Samples in Solid-State NMR. J Phys Chem C 122:16437–16442. doi: 10.1021/acs.jpcc.8b05600

Zhao W, Fernando LD, Kirui A, et al (2020) Solid-state NMR of plant and fungal cell walls: A critical review. Solid State Nucl Magn Reson 107:101660. doi: 10.1016/j.ssnmr.2020.101660

Zhou DH, Rienstra CM (2008) High-performance solvent suppression for proton detected solid-state NMR. J Magn Reson 192:167–172. doi: 10.1016/j.jmr.2008.01.012

Zhou DH, Shah G, Mullen C, et al (2009) Proton-detected solid-state NMR spectroscopy of natural-abundance peptide and protein pharmaceuticals. Angew Chemie - Int Ed 48:1253–1256. doi: 10.1002/anie.200801029

Zinke M, Fricke P, Samson C, et al (2017) Bacteriophage Tail-Tube Assembly Studied by Proton-Detected 4D Solid-State NMR. Angew Chemie - Int Ed 56:9497–9501. doi: 10.1002/anie.201706060